Synergistic Control of Mesenchymal Stem Cell Differentiation by Nanoscale Surface Geometry and Immobilized Growth Factors on TiO_2 Nanotubes

*Jung Park, Sebastian Bauer, Andreas Pittrof, Manuela S. Killian, Patrik Schmuki, and Klaus von der Mark**

The aim of this study is to elucidate whether combined environmental signals provided by nanoscale topography and by growth factors control cell behavior of mesenchymal stem cells (MSCs) in a synergistic or simply additive manner. Chondrogenic and osteogenic differentiation of MSCs is studied on vertically aligned TiO_2 nanotubes of size 15 and 100 nm with and without immobilized bone morphogenetic protein-2 (BMP-2). Although BMP-2 coating stimulates both chondrogenic and osteogenic differentiation of MSCs, the response strongly depends on the surface nanoscale geometry of the BMP-2-coated nanotubes. Chondrogenic differentiation is strongly supported on 100 nm BMP-2-coated nanotubes, but not on 15 nm nanotubes, which induce spreading and de-differentiation of chondrocytes. A similar response is observed with primary chondrocytes, which maintain their chondrogenic phenotype on BMP-2-coated 100 nm nanotubes, but de-differentiate on 15 nm nanotubes. In contrast, osteogenic differentiation is greatly enhanced on 15 nm but not on 100 nm BMP-2-coated nanotubes as shown previously. Furthermore, covalent immobilization of BMP-2 rescues MSCs from apoptosis occurring on uncoated 100 nm TiO_2 nanotube surfaces. Thus, combined signals provided by BMP-2 immobilized to a defined lateral nanoscale spacing geometry seem to contain environmental cues that are able to modulate a lineage-specific decision of MSC differentiation and cell survival in a synergistic manner.

Dr. J. Park,[+] Prof. K. von der Mark
Department of Experimental Medicine I
Nikolaus-Fiebiger-Center of Molecular Medicine
Friedrich-Alexander-University of Erlangen-Nuremberg
Glueckstrasse 5, 91054 Erlangen, Germany
E-mail: kvdmark@molmed.uni-erlangen.de
Dr. J. Park
Department of Pediatrics
Division of Molecular Pediatrics
University Hospital Erlangen
91054 Erlangen, Germany
Dr. S. Bauer,[+] A. Pittrof, M. S. Killian, Prof. P. Schmuki
Department of Materials Science
Institute for Surface Science and Corrosion (LKO)
Friedrich-Alexander-University of Erlangen-Nuremberg
Martensstrasse 7, 91058 Erlangen, Germany
[+] These authors contributed equally to this work.

DOI: 10.1002/smll.201100790

1. Introduction

Cell differentiation events and lineage decisions occurring during embryonic development, wound healing, or tissue repair are controlled in a synergistic manner by soluble growth factors and hormones on the one hand, and stationary factors including the extracellular matrix (ECM) and cell–cell interactions on the other.[1–3] Recently, there is also increasing evidence that the elasticity and resilience of the ECM are important parameters in determining cell differentiation as well as cell adhesion and growth.[4,5] Furthermore, numerous studies using synthetic biomaterials and biomimetic surfaces modified by nanoporous[6,7] and nanoprotrusive surface topography[8] and nanoscale surface lithography[9,10] have revealed that not only the surface chemistry but also the nanoscale surface topography are primary determinants of cellular responses to surfaces, including adhesion,

small NANO MICRO

proliferation, migration, and differentiation (for a review, see von der Mark et al.[11]). Therefore, nanoscale surface modifications on biomimetic materials are receiving increasing attention in tissue engineering, for example, in the development of biomimetic materials for vascular grafts, stents, or bone implants. The aim is to design biomaterials which provide an extracellular microenvironment that is not only biocompatible, but also is able to promote the recapitulation of developmental processes for organ- and tissue-specific differentiation.[12,13] Although abundant information exists on individual regulatory pathways controlled by growth factors, hormones, cytokines, and their receptors, current tools are as yet insufficient to decipher and integrate multiple synergistic effects including biomechanical signals, topographic information, and signals received from the ECM or cell surface contacts. How cells exactly respond to complex signals elicited by the nanoscale-modified matrix in concert with growth factors, and cell–matrix and cell–cell interactions is still elusive.

Previously, we have shown that adhesion, migration, and proliferation of mesenchymal stem cells (MSCs) as well as their differentiation to osteoblasts are strongly dependent on surface topography at the nanoscale; a maximum of cell adhesion, proliferation, migration, and differentiation was observed on vertically aligned TiO_2 nanotubes 15 nm in diameter, while 100 nm nanotubes induced apoptosis.[14–16] Differentiation of MSCs to osteoblasts or chondrocytes in vitro and in tissue regeneration can be specifically regulated by a combination of growth factors and culture conditions. Osteogenic differentiation is induced by Vitamin D3, bone morphogenetic protein-2 (BMP-2) or BMP-3 (osteogenin), β-glycerophosphate, and ascorbate,[17–19] while transforming growth factor $\beta 3$ (TGF$\beta 3$; low serum), BMP-2, insulin-like growth factor (IGF), and—importantly—nonadhesive culture conditions promote chondrogenic differentiation.[20,21] Thus, BMP-2 is a potent morphogen inducing both osteogenic and chondrogenic differentiations from mesenchymal stem/progenitors in vitro and in vivo. During several decades, BMP-2 has been widely applied for bone and cartilage tissue engineering[22–26] as well as for improved osseous integration of the bone/implant interface[27–31] in several experimental animal models and clinical trials.

Surface modification by immobilizing adhesive peptides, growth factors, or hormones onto biomaterial surfaces via either chemicals or a physical tool has proven a valuable method to improve specific cell and tissue responses at the implant/cell–tissue interface.[32,33] In the present study, we generated TiO_2 chips with nanotubular surface topography to which BMP-2 was covalently immobilized with carbonyldiimidazole (CDI). We investigated 1) whether immobilized BMP-2 is functionally active to promote MSC differentiation, and 2) whether there are synergistic effects of signals from immobilized BMP-2 on the one hand, and from nanoscale lateral spacing geometry on the other hand in regulating the lineage decisions of MSCs beyond the additive effects of each single parameter.

Herein, we present a reductionistic approach to gain insight into potential synergistic effects of two types of environmental information: growth factors and nanoscale surface topography. Our results show that BMP-2 immobilized in a distinct adhesive surface topography has a significantly stronger impetus on chondrogenic versus osteogenic differentiation than each signal by itself or the additive effects of both. Chondrogenic differentiation of MSCs was several-fold enhanced on BMP-2-coated 100 nm nanotubes as compared to uncoated 100 nm nanotubes, or on compact surfaces coated with BMP-2 only. In contrast, osteogenic differentiation of MSCs was strongly enhanced on 15 nm BMP-2-coated nanotubes in comparison to cultures on uncoated 15 nm nanotubes or to cultures on BMP-2-coated 100 nm nanotubes.

2. Results

Previously we have shown that vitality, proliferation, and motility in several types of adherent cells including MSCs, primary osteoblasts, osteoclasts, and endothelial cells are critically influenced by nanoscale TiO_2 surface topography in the sub-100-nm range.[14,15,34] As a hypothetical model, we have proposed that a spacing of less than 30 nm with a maximum at 15 nm provided an effective length scale for accelerated integrin clustering/focal contact formation of MSCs compared to smooth TiO_2 and larger diameters of nanotubes including 100 nm.[14] In the present study using human and rat MSCs (Supporting Information Figure S1a), initial cell adhesion behavior on BMP-2-immobilized surfaces was evaluated. TiO_2 nanotubes 15 or 100 nm in diameter were activated with CDI, which binds to the terminal hydroxyl groups of TiO_2. After incubation with recombinant BMP-2 (100 ng mL^{-1}), BMP-2 bound covalently to CDI through amino groups (**Figure 1**a). Coupling efficiency was determined by time-of-flight secondary ion mass spectrometry (TOF-SIMS) analysis (Figure 1b–e). TOF-SIMS signals showed a systematic assignment of typical fragments of amino acids according to their mass spectral signals. The CDI signal (the peak at *m/z* 67.03 u, Figure 1b, TiC) was immediately substituted by BMP-2-specific signals (TiCB). Several characteristic amino acid ratios characteristic for BMP-2, such as valine/proline, glutamine, lysine/leucine, and histidine, were displayed on CDI/BMP-2 covalent bound surfaces (TiCB, Figure 1c–e). Furthermore, a successful coupling of BMP-2 to CDI-activated TiO_2 nanotubes was shown by immunostaining after two washing steps with an anti-BMP-2-specific antibody (**Figure 2**a,b), while almost all BMP-2 was washed away from nonactivated TiO_2 nanotubes (Figure 2a, lower panels). After BMP-2 immobilization, the nanotubular topography was well preserved without any evidence of nanotube blocking by the CDI–BMP-2 complex, as shown by scanning electron microscopy (SEM; Figure 1f).

In accordance with our previous findings, 15 nm nanotubes promoted cell adhesion of both human and rat MSCs more strongly than 100-nm-diameter nanotubes, irrespective of immobilized BMP-2 (Figure 2c,d) or immobilized bovine serum albumin (BSA) as a control (Supporting Information Figure S1b). This result indicated a dominant effect of nanoscale surface topographic modification on cell adhesion, which is consistent with previous reports on nanoprotrusive models in distinct spacing distances of gold nanodots with RGDfK

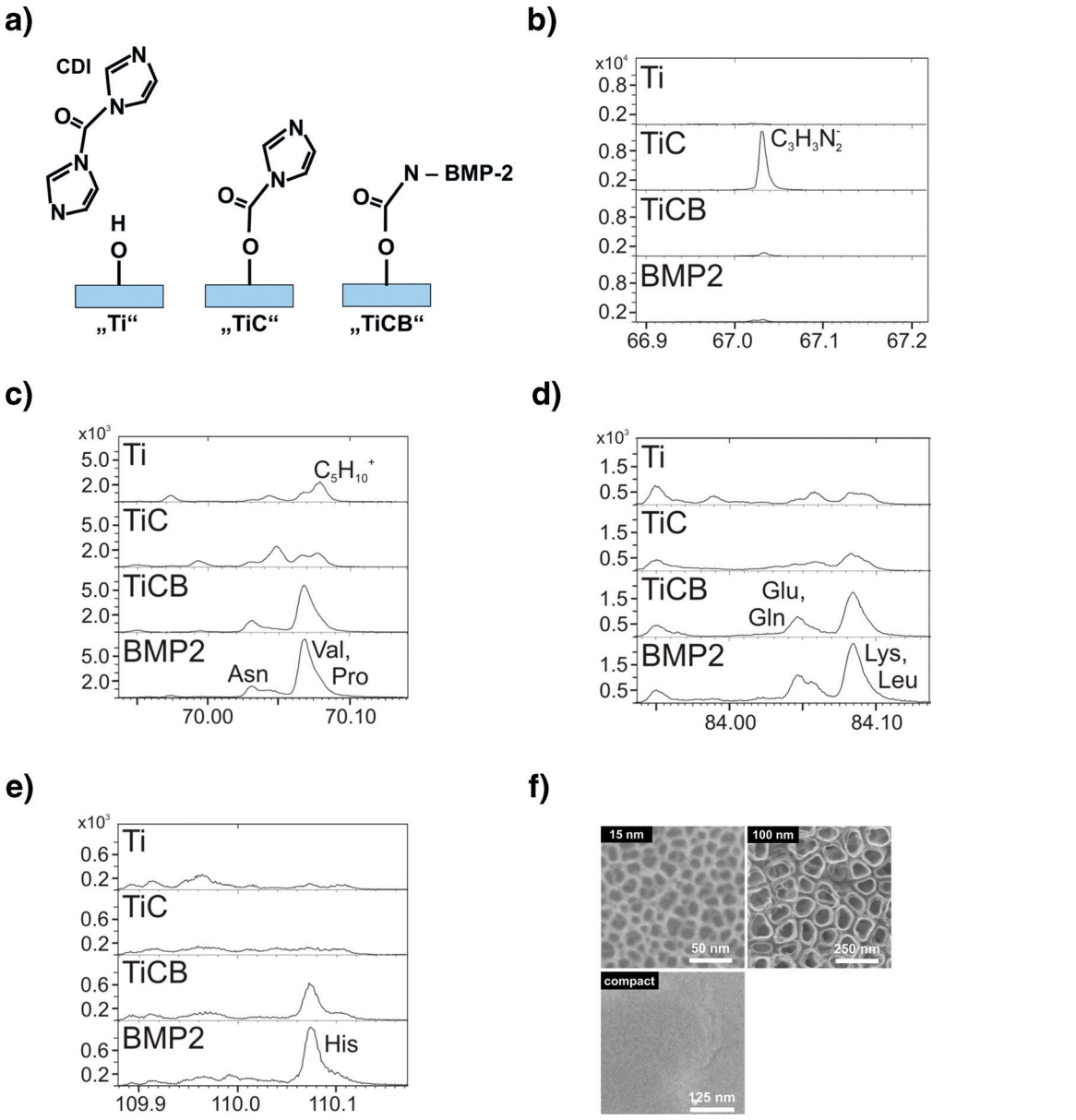

Figure 1. BMP-2 immobilization by CDI coupling on nanotube layers. a) Schematic illustration of BMP-2 immobilization by covalent reaction of an amino group of the protein with the grafted CDI. b–e) TOF-SIMS provided confirmation of the attached BMP-2 proteins on the surface with the specific fragment pattern generated by amino acids. Representative sections of the TOF-SIMS spectra are shown for the bare TiO_2 substrate (Ti), CDI-treated TiO_2 (TiC), BMP-2 attached on TiO_2 via CDI (TiCB), and a droplet of BMP-2 solution, which was dried on the substrate for reference purposes (BMP-2). b) The attachment sequence shows an intense signal in the negative spectra at $C_3H_3N_2^-$ (m/z 67.03 u) for the region of CDI (TiC); this signal disappears nearly completely after attachment of BMP-2 (TiCB), indicating that CDI is substituted by BMP-2. c–e) Characteristic amino acid fragments for BMP-2 are displayed: c) valine (m/z 70.07 u: $C_4H_8N^+$); d) glutamine, glutamic acid (m/z 84.04 u: $C_4H_6NO^+$), and lysine, leucine (m/z 84.08 u: $C_5H_{10}N^+$); and e) histidine (m/z 110 u: $C_5H_8N_3^+$). f) SEM images of TiO_2 nanotube surfaces with 15 and 100 nm diameters and compact oxide surface used as reference after BMP-2 immobilization prove that the surface structures were clearly maintained without any evidence of blocking the nanotubes by the CDI–BMP-2 complex.

coating[9] and nanoscale roughness on silicon or silica substrates.[35,36] Although MSCs on BMP-2-immobilized surfaces of 100 nm nanotubes revealed an elongated cell morphology similar to that on 15 nm nanotubes without CDI coupling (Figure 2c, right panels), cell adhesion efficiency on BMP-2-coated and uncoated 100 nm nanotubes was far below the adhesion rates on 15 nm nanotubes. Thus, BMP-2 itself did not seem to affect adhesion efficiency or cell proliferation, which is consistent with the notion that BMP-2 itself is a potent inducer of cell differentiation rather than a mitogenic effector or adhesive protein.

Rather notable effects of immobilized BMP-2 on nanotubes were noticed in rescuing cells from apoptosis on 100 nm nanotubes. As reported previously,[14] on uncoated 100 nm nanotubes human and rat MSCs undergo extensive programmed cell death after 2 days, as determined by FACS analysis after annexin V staining (Figure 2e,f) and cleaved caspase-3 immunostaining (Supporting Information Figure S2).

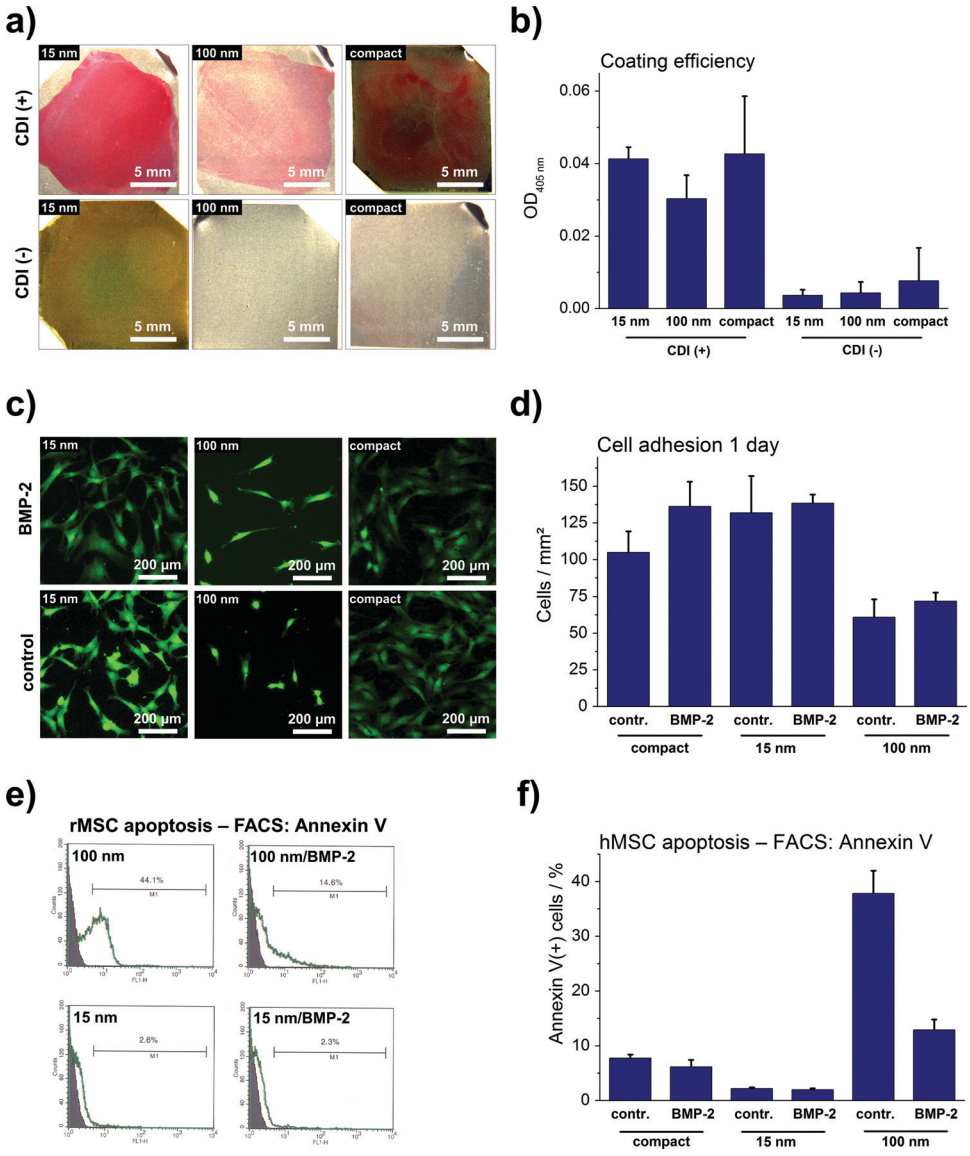

Figure 2. MSC responses to BMP-2 immobilized on TiO_2 nanotube surfaces. a) Detection of covalently immobilized BMP-2 on CDI-activated surfaces by immunohistochemical staining with anti-BMP (upper panels) compared to unmodified surfaces (lower panels). b) Quantitative measurement of bound BMP-2 showed stable binding of BMP-2 to TiO_2 nanotubes 15 and 100 nm in diameter and compact oxide layers after two washing steps. c,d) Adhesion of green fluorescent protein (GFP)-labeled rat MSCs to BMP-2-coated and uncoated surfaces of 15- and 100-nm-diameter nanotubes and compact oxide surfaces used as reference. BMP-2 had no effect on adhesion rates, which were significantly higher on 15 nm than 100 nm nanotubes. e,f) Rat MSCs (rMSCs) underwent high rates of apoptosis on 100 nm nanotubes 2 days after plating, but not on 15 nm uncoated nanotubes. Fluorescence-activated cell sorting (FACS) analysis after annexin V staining of human MSCs (hMSCs) showed that apoptosis on 100 nm nanotubes was rescued on immobilized BMP-2 surfaces. OD=optical density.

BMP-2 immobilized on 100 nm nanotubes, however, strongly reduced the number of apoptotic cells (Figure 2e, upper panels, and Supporting Information Figure S2, middle panel). This finding is consistent with reports showing that BMP-2 can work as an anti-apoptotic signal inducer.[37,38]

The most remarkable finding, however, was that BMP-2 stimulated the differentiation of MSCs to chondrocytes on 100 nm nanotubes but not on 15 nm nanotubes. On BMP-2-coated 100 nm nanotubes MSCs rounded up and formed large aggregates, which underwent chondrogenic differentiation after 5–7 days, as determined by immunofluorescence staining for the cartilage-specific collagen II (**Figure 3**a, left panels). On uncoated 100 nm nanotubes, however, only a few collagen II positive cells were seen (Figure 3a, right panels). Also, on 15 nm nanotubes, chondrogenic differentiation was strongly impaired, even on BMP-2-coated surfaces (Figure 3a, left panels). Similarly, differentiated primary mouse chondrocytes maintained their chondrocyte cell morphology and continued to highly express collagen II on 100 nm BMP-2-coated nanotubes, but not on 15 nm BMP-2-coated nanotubes (Figure 3c, left panels, and Supporting

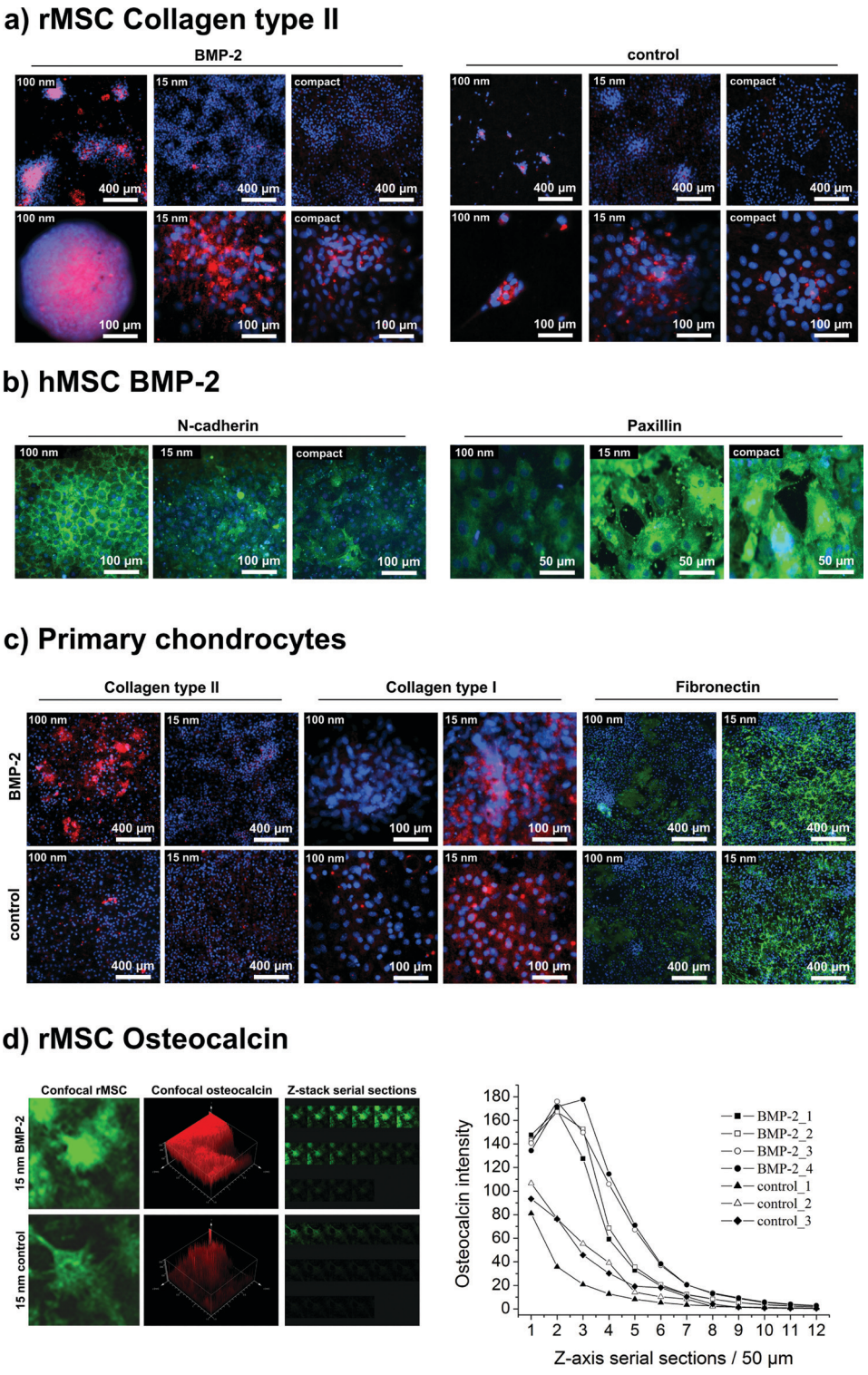

Figure 3. Chondrogenic and osteogenic differentiation of MSCs in response to combined microenvironmental signals of BMP-2 and nanoscale spacing distances. a) Chondrogenic differentiation of rat MSCs as indicated by type II collagen staining and nodule formation was strongly supported on BMP-2-coated 100 nm nanotubes, but much less on 15 nm nanotubes (left panels). Only minor chondrogenic differentiation was seen on uncoated 15 and 100 nm nanotubes (right panels). b) Human MSCs on 100 nm nanotubes with BMP-2 showed strongly enhanced cell–cell contacts, as indicated by N-cadherin staining (left panel), but almost no focal contact formation shown by paxillin staining (right panel). In contrast, MSCs did not develop cell–cell contacts on 15 nm nanotubes, but intense paxillin-positive focal adhesion contacts. c) Primary mouse chondrocytes maintained the chondrocyte phenotype on BMP-2-coated but not on uncoated 100 nm nanotubes (left panel), but de-differentiated on 15 nm nanotubes as indicated by loss of type II collagen and onset of abundant type I collagen and fibronectin staining (middle and right panels). d) Differentiation of MSCs to osteoblasts was strongly supported on 15 nm BMP-2-coated nanotubes but much less on uncoated nanotubes as indicated by osteocalcin staining. No osteogenic differentiation occurred on 100 nm nanotubes (results not shown, see Park et al.[14]). Osteocalcin fluorescence along the *z* -axis of cells was monitored by confocal laser scanning microscopy.

small NANO MICRO

Information Figure S3). In other words, chondrogenic differentiation could be strongly promoted by the combination of the two signals.

There is ample evidence that chondrogenesis of limb bud mesenchymal cells is proceeded by a cell condensation process with increasing cell–cell contacts, marked by enhanced expression of N-cadherin.[39] In fact, analyzing N-cadherin expression in MSCs on BMP-2-coated 100 nm nanotubes, the surface which most strongly promoted chondrogenic differentiation, revealed a high density of N-cadherin-positive cell–cell contacts (Figure 3b, left panels), while no cell–cell contacts were observed on BMP-2-coated 15 nm nanotubes (Figure 3b). In contrast, intense paxillin staining on 15 nm nanotubes confirmed extensive integrin-mediated focal contact formation (Figure 3b, right panels), which is not compatible with cell condensation and chondrogenic differentiation. A similar response was observed with primary chondrocytes, which maintained their chondrogenic phenotype on BMP-2-coated 100 nm nanotubes including type II collagen expression (Figure 3c, left panels), but de-differentiated on 15 nm nanotubes as indicated by abundant type I collagen and fibronectin expression (Figure 3c, middle and right panels).

Osteogenic differentiation of MSCs, however, was regulated in the opposite manner. As shown previously, cell adhesion, proliferation, and osteogenic differentiation of MSCs were stimulated best on 15 nm nanotubes.[14,15] This was confirmed here: only on 15 nm but not on 100 nm surfaces was differentiation of MSCs to osteoblasts observed, as indicated by staining for osteocalcin (Figure 3d). While osteogenic differentiation also occurred on uncoated surfaces, the extent of differentiation was significantly enhanced on BMP-2-coated nanotubes (Figure 3d, lower panel).

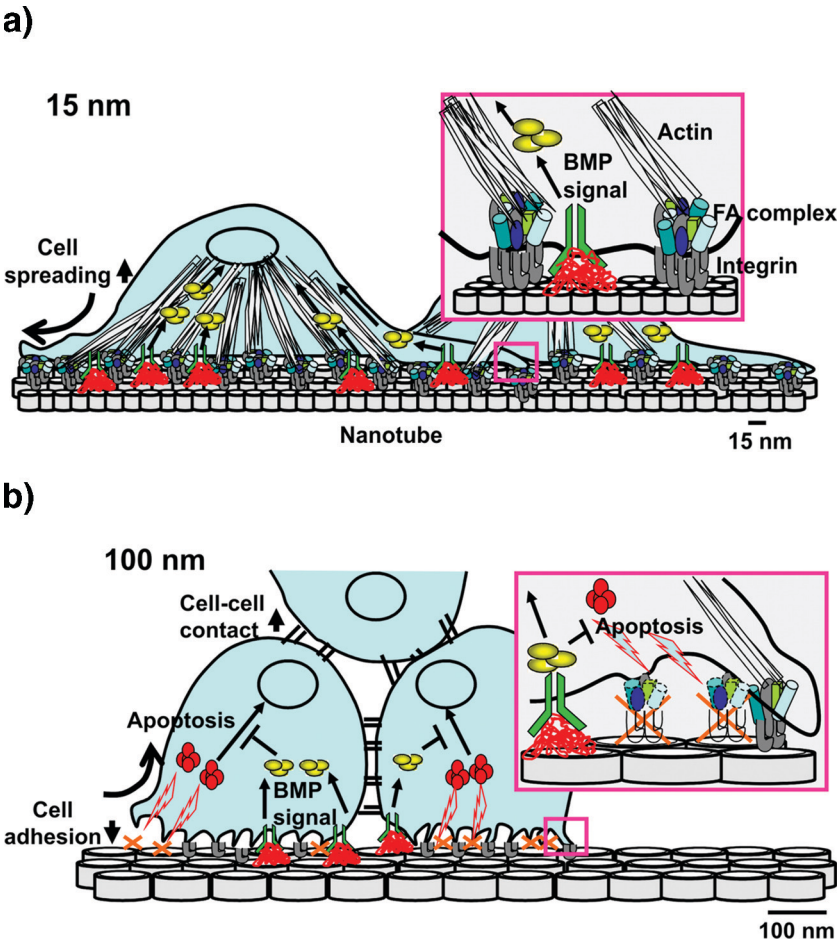

Figure 4. Model for synergistic control of MSC differentiation by nanoscale surface geometry and immobilized growth factors. a) Intense integrin clustering and focal contacts are supported on a 15 nm lateral spacing microenvironment in synergy with BMP-2 signaling, inducing cell spreading, actin polymerization, and osteogenic differentiation of MSCs. b) Larger lateral spacing on 100 nm nanotubes does not support stable cell adhesion, cell spreading, and focal contact formation, but enhanced cell–cell contacts, thereby causing aggregate formation, rounded cell shape, and supporting chondrogenic differentiation. Immobilized BMP-2 stimulates chondrogenic differentiation and protects cells from programmed cell death (apoptosis).

This strictly nanospacing-controlled direction of MSCs into osteogenic versus chondrogenic differentiation, as well as the apparently "unspecific" support of both differentiation pathways by BMP-2, may appear surprising at first glance. Concerning the bifunctional role of BMP-2, however, this is in line with the multiple roles of BMP-2 and other BMP factors in development, not only in osteogenesis and chondrogenesis,[40,41] but also in nerve and muscle development, or in the development of the immune system and others.[42–44] Like most other growth and developmental control factors, BMP-2 may induce differentiation of different cell types depending on the cellular context of BMP receptors, intracellular signaling pathways besides the SMAD regulated pathways, and synergistic effects of other growth factors.

Figure 4 depicts a model showing how the combined environmental signals provided by nanoscale topography and by growth factors may control the cell behavior of MSCs in a synergistic manner. Intense integrin clustering and focal contacts provided by a 15 nm lateral spacing microenvironment may stimulate osteogenic differentiation of MSCs synergistically with BMP-2 signaling (Figure 4a), while anti-apoptotic effects of BMP-2 may protect cells from programmed cell death evoked by failure of proper cell adhesion on larger lateral spacings, for example, on 100 nm nanotubes (Figure 4b). On the other hand, 100 nm nanotubes supporting enhanced cell–cell contacts rather than cell–substrate contacts induce cell aggregation, which promotes chondrogenic differentiation in the presence of BMP-2.

3. Discussion

The stimulation of osteogenic differentiation by a 15 nm nanospacing is in accordance with previous findings[14,15] and may be explained on the basis of our observation of enhanced focal contacts, enhanced stress fibers, and integrin-mediated paxillin phosphorylation of MSCs on 15 nm nanotubular surfaces. We hypothesized that the 15 nm nanospacing, which corresponds approximately to the size of the extracellular ligand binding domains of integrin dimers, enforces clustering of integrins, which triggers intracellular signaling, actin stress fiber formation, and finally differentiation.[9,10,14,15]

In contrast, chondrogenic differentiation is mostly achieved under conditions which minimize formation of focal contacts and stress fibers but allow cell aggregation, such as culture in soft agar or soft collagen gels, or micropellet culture in suspension.[45–47] The onset of chondrogenesis in developing long bones is characterized by cell condensation, reduction of intercellular spaces, and establishment of extensive cell–cell contacts between mesenchymal chondrogenic cells.[48,49] Accordingly, the assembly of extracellular cartilage matrix by differentiated chondrocytes in vitro is supported under the nonadhesive conditions described above, while prolonged culture of chondrocytes in monolayer culture results in loss of the differentiated phenotype. Chondrocytes plated on adhesive surfaces tend to change morphology to fibroblastic, flattened cells, cease production of type II collagen and aggrecan, and synthesize type I and type III collagen instead.[50–52] This process is initiated by the formation of enhanced focal contacts and stress fibers, while in rounded, differentiated chondrocytes actin filaments are assembled into a cortical filamentous network.[53] A strict correlation between chondrocyte phenotype and actin filament assembly has been concluded from a study which showed that dissolving actin stress fibers in fibroblastic, de-differentiated chondrocytes by cytochalasin B caused re-differentiation of the cells to hyaline, rounded chondrocytes.[54]

Thus, in contrast to most other tissue cells, a strong adhesive response, such as provided by 15 nm nanotubular TiO_2 surfaces enforcing the formation of focal contacts and stress fibers, is not compatible with the expression of the chondrogenic phenotype. A surface topography not supporting the formation of focal contacts such as 100 nm nanotubes,[14] however, promotes cell rounding and formation of cell–cell contacts which favor chondrogenic differentiation instead of cell–matrix contacts. Spherical, differentiated hyaline chondrocytes also interact with the surrounding extracellular cartilage matrix through integrins,[55–57] but these integrins are not involved in focal contacts and do not induce stress fibers. Thus, only under such nonadhesive conditions does BMP-2 seem able to induce chondrogenic differentiation, which indicates the dominance of surface nanoscale topography over growth factor effects in this case.

Recently, encouraging results have been achieved using recombinant BMP-2 for cartilage and bone regeneration in animal experiments and clinical applications, but several problems such as high cost, relatively high protein doses from several micrograms up to milligrams, as well as a short protein half-life are obstacles that still have to be overcome. Recently, in reconstructive dental and orthopedic surgery, various attempts have been made to modify the structure of the implant surface to enhance osseous integration of the bone/implant interface. Considering the fact that very low amounts (0.5 ng cm^{-2} of each sample) of BMP-2 used for immobilization via CDI coupling on nanotubes were sufficient to stimulate osteogenic and chondrogenic differentiation, surface coating with BMP-2 via CDI on nanotubes seems an efficient alternative to administration of high doses of recombinant BMP-2 in vivo.

Recent studies on nanoscale topological arrangement by fabrication of ordered TiO_2 nanotube layers with a self-organization process[6,58–60] and other nanoscale surface geometry designs[12,35,61,62] have been driving strategies of implant surface modifications from the micrometer into the nanometer scale, and have opened a new avenue directing nanoscale biomimetic surface optimization by novel coating strategies. The approach presented here using two factor modulations, namely immobilized growth factor and nanoscale modification of topography on TiO_2 nanotubes for directing cell development into different lineages, bears the potential for multiple modifications of implant surfaces and may stimulate endeavors for the improvement of further nanoscale biomimetic surfaces in tissue engineering.

4. Conclusion

The data indicate that BMP-2 immobilized on TiO_2 surfaces with defined nanoscale topography provided by nanotubular structures of defined size may elicit specific signals for lineage-specific differentiation of MSCs towards osteogenic or chondrogenic lineages.

5. Experimental Section

TiO_2 Nanotube and Compact Oxide Layer Formation: Titanium foils (99.6% purity, Advent Ltd.) were used as substrates for the anodic growth of compact oxide and TiO_2 nanotube layers. For anodization an electrochemical cell with a three-electrode configuration was used. Platinum gauze served as a counter electrode and a Haber–Luggin capillary with Ag/AgCl (1 M KCl) electrode was used as a reference electrode. For electrochemical experiments a high-voltage potentiostat (Jaissle IMP 88-200 PC) was used. Electrochemical treatments were carried out according to previously reported work[59] in 1 M H_3PO_4 without (compact oxide layers) and with (nanotube layers) addition of 0.12 M HF. For nanotube formation potentials of 1 and 20 V at room temperature were applied and resulted in nanotube diameters of 15 and 100 nm as shown in Figure 1f.[59] For compact TiO_2 surfaces as reference, titanium foils were anodized in fluoride-free 1 M H_3PO_4 at 20 V for 15 min. All electrolytes were prepared from reagent-grade chemicals and deionized water.

After electrochemical treatment, the samples were immersed in deionized water for at least 2 days to reduce the content of residual fluorides to values less than 2 at% in the grown oxide structures, as shown in previous work.[34] It was shown that residual fluoride contents varying between approximately 0 and 8 at% did not significantly influence cell behavior.[34] All samples were sterilized

using an autoclave at 121 °C prior to cell seeding. High-resolution X-ray diffraction (XRD) of the nanotube layers after autoclaving showed the tubes had an amorphous nature, as shown in previous work.[34] For morphological characterization of sample surfaces, a field-emission scanning electron microscope (FE-SEM, S-4800, Hitachi) was used.

Covalent Immobilization of BMP-2: Before surface modification with *N*,*N*-carbonyldiimidazole (CDI) the samples were washed in acetone, ethanol, and ultrapure water (each step for 5 min), followed by exposure to UV light with the addition of water using a high-power Hg lamp (UV irradiation 15 W cm^{-2}) for 30 min for cleaning purposes. The grafting of BMP-2 onto the oxide surfaces was achieved by binding CDI (Aldrich) covalently. Therefore, a solution (25 μM) of CDI in chloroform was used. All samples were held for 12 h in the CDI/chloroform solution. Then the samples were taken out, subsequently washed with chloroform for 10 min each under ambient stirring, and dried at 70 °C overnight. For covalent grafting with BMP-2, a droplet (50 μL) of phosphate-buffered saline (PBS) with physiologically relevant concentrations of the protein (final concentration of BMP-2, 100 ng mL^{-1}, 0.5 ng cm^{-2} each sample) was pipetted onto each surface and kept at 37 °C for 6 h.

Time-of-Flight Secondary Ion Mass Spectrometry: TOF-SIMS provides information about chemical structures within the protein and consequently can be used as a tool for surface protein analysis. The fragment pattern generated by amino acids allows the confirmation of attached proteins on surfaces and thus it is possible to distinguish specific proteins.[63–65] Positive and negative static SIMS measurements were performed on a TOF-SIMS instrument (TOF-SIMS 5 spectrometer, ION-TOF). The samples were irradiated with a pulsed 25 keV Bi^{3+} liquid-metal ion beam. Spectra were recorded in the high mass resolution mode ($m/\Delta m >$ 8000 at ^{29}Si). The beam was electrodynamically bunched down to <1 ns to increase the mass resolution and rastered over a 500 × 500 μm^2 area. The primary-ion dose density (PIDD) was kept at 5×10^{11} ions cm^{-2}, thereby ensuring static conditions. Signals were identified using the accurate mass as well as their isotopic pattern. Poisson correction was used for integration of the signal intensities.[66]

Immunohistochemical Staining for Immobilized BMP-2: Recombinant BMP-2 protein (100 ng mL^{-1}) was plated at a volume of 50 μL on each sample (1.5 cm × 1.5 cm in size), incubated for 6 h at 37 °C, and washed twice with PBS. Then each sample was incubated with antibodies of rabbit polyclonal anti-BMP-2 (Santa Cruz) for 1 h. After washing three times with PBS for 5 min each, the samples were washed with PBS twice for 5 min, incubated further with a 1:250 dilution of the secondary antibody (DAKO, biotinylated polyclonal goat anti-rabbit antibody), and further incubated with streptavidin–alkaline phosphatase complex for 45 min followed by fast red staining (Sigma, SIGMAFAST Fast Red TR/Naphthol AS-MX tablets) after washing with PBS (three times for 10 min each step). Following washing three times with PBS, BMP-2 staining images were taken using an Axiovert 2000 ApoTome microscope with an AxioCam digital camera and AxioVision software (Zeiss).

Cell Culture: Human MSCs from fresh umbilical cord blood (UCB) samples were isolated and expanded as previously described.[67] The mononuclear cell fraction from fresh UCB samples was isolated by density gradient centrifugation using Ficoll-Paque Plus (Amersham Biosciences) according to the manufacturer's protocol. CD133+ cells were obtained by incubating the cells with a microbead anti-CD133 antibody (AC133, Miltenyi Biotech) followed by separation on a MACS cell sorter (Miltenyi Biotech). The purified mononuclear cells were plated at a density of 1×10^5 cm^{-2} in expansion medium containing hematopoietic progenitor cell expansion medium (Promocell) including recombinant human TPO, SCF, flt3-ligand, and IL-3 and cells were cultured for 2 weeks. Afterward, nonadherent cells were washed out and adherent cells were further cultured with 60% Dulbecco's modified Eagle's medium low glucose (DMEM-LG; Gibco BRL), 40% MCDB-201 (Sigma), epidermal growth factor (Sigma) and PDGF-BB (R&D Systems), both at a concentration of 10 ng mL^{-1}, human recombinant protein LIF (1000 units mL^{-1}), 1× insulin–transferrin–selenium, 1× linoleic acid–bovine serum albumin (LA-BSA), dexamethasone (10^{-9} M; Sigma), ascorbic acid 2-phosphate (10^{-4} M; Sigma), 100 units of penicillin/streptomycin, and 20% fetal calf serum (FCS; Hyclone Laboratories) on plates coated with fibronectin (100 ng mL^{-1}). The medium was changed every third day and cells were cultivated up to 6 weeks after cell plating. The expanded cells were then trypsinized and single clonal cells were obtained by limiting dilution and further expanded.

Rat MSCs were isolated and expanded from fresh bone marrow from femurs of 4-week-old Wistar rats as described previously,[14,68] and selected clonal cells were further expanded in medium containing 60% DMEM-LG (Gibco BRL), 40% MCDB-201 (Sigma) and supplemented with 1× insulin–transferrin–selenium (Sigma), 1× LA-BSA (Sigma), 10^{-9} M dexamethasone (Sigma), 10^{-4} M ascorbic acid 2-phosphate (Sigma), 100 units of penicillin, 1000 units of streptomycin (Gibco), EGF (10 ng mL^{-1}, Sigma), PDFG-BB (10 ng mL^{-1}, R&D Systems), 1000 units mL^{-1} rat LIF (Chemicon), and 2% FCS (Hyclone Laboratories). The expanded cells showed multipotent potential to differentiate into multiple mesenchymal lineages including osteoblast, chondroblast, adipocyte, myoblast, myofibroblast, and endothelial cells in differentiation experiments in vitro. For cell adhesion and differentiation assay, GFP-labeled MSCs were used following infection with retroviruses containing a green fluorescent protein (GFP) cDNA and isolation of a stably GFP-expressing clone. For each experiment cells were trypsinized and plated on each different size of nanotube or compact surface at cell densities as indicated in DMEM/MCDB-201 medium mix as described above with 2% FCS without growth factors.

Primary chondrocytes were obtained from femur cartilage tissue of 4-day-old newborn mouse and plated with F12/DMEM containing 1× insulin–transferrin–selenium (Sigma) and 10% FCS. Cell adherence was allowed for 10 days and afterwards grown cells at subconfluency were used for the experiments.

For osteogenic differentiation, cells were plated at the cell density of 50 000 cm^{-2} in alpha medium (Invitrogen) containing 10% FCS. Five days after cell plating the culture medium was changed to differentiation medium containing 10% FCS, dexamethasone (100 nM), β-glycerophosphate (10 mM), and ascorbic acid (50 μg mL^{-1}). The cells were cultivated for 2 weeks and analyzed by immunocytochemistry and quantitative mineralization assay.

For chondrogenic differentiation, cells were plated at the cell density of 50 000 cm^{-2} in F12/DMEM containing 1× insulin–transferrin–selenium (Sigma) and 10% FCS. The culture medium was replaced every 2 days in all experiments.

Cell Adhesion and Apoptosis Assay: For cell experiments a BMP-2 droplet (50 μL) with PBS at a final concentration of 100 ng mL^{-1}

was pipetted onto each surface (compact layer, 15 or 100 nm nanotube surface) with CDI modification and kept at 37 °C for 6 h, followed by washing with PBS twice for cell plating. Samples without CDI/BMP-2 coatings were used as controls.

GFP-labeled MSCs were plated on TiO_2 surfaces with cell densities of 5000 cm^{-2}. For cell adhesion experiments, 24 h after cell plating adherent cells were counted at six different areas (1280 × 1024 pixels), and each sample was depicted under a fluorescence microscope. Cell count analysis was evaluated by three individuals and values were combined to one mean and standard deviation for each specimen. Images were taken using an Axioplan 2 microscope equipped with an AxioCam digital camera and AxioVision software (Zeiss).

Cell apoptosis assays were performed by resuspending the cells 2 days after plating with a cell density of 50 000 cm^{-2} in binding buffer (100 µL, 10 mM 4-(2-hydroxyethyl)-1-piperazineethanesulfonic acid (HEPES), pH 7.4, 140 mM NaCl, 2.5 mM $CaCl_2$), followed by incubation with annexin V (5 µL) conjugated with fluorescein isothiocyanate (FITC, a kind gift of Dr. Ernst Pöschl, Erlangen) for 15 min at room temperature in the dark. Propidium iodide was added immediately before analysis to exclude necrotic cells. Annexin V-positive cells were counted using a fluorescence-activated cell sorter.

Immunocytochemistry: For immunofluorescence staining, the cells on each sample were fixed with 4% paraformaldehyde for 10 min and permeabilized with 0.2% Triton X-100 in PBS to allow intracellular staining. The samples were blocked with protein blocking solution (DAKO) and incubated with mouse monoclonal anti-type I collagen (Santa Cruz), anti-type II collagen, anti-N-cadherin, anti-paxillin (Signal Transduction), anti-osteocalcin (Takara) or rabbit polyclonal anti-cleaved caspase-3 (Cell Signaling) for 1 h at room temperature. After washing away any unbound primary antibody with PBS twice for 5 min, the samples were incubated further with a 1:250 dilution of the secondary antibody (either goat anti-mouse Cy5-conjugated (Chemicon, 1:300) or anti-mouse FITC-conjugated antibody (Jackson Immunoresearch, 1:200) or anti-rabbit Cy5-conjugated antibody (Cell Signaling, 1:500)) for 30 min at room temperature. Following washing with PBS (three times for 10 min) the cells were analyzed by fluorescence microscopy using an Axioplan 2 microscope (Zeiss). Cell nuclei were stained blue with 4',6-diamidino-2-phenylindole (DAPI; Roth).

For immunoassay using type II collagen, the samples were incubated with biotinylated anti-mouse secondary antibody for 1 h at room temperature following primary antibody incubation as described above. After washing away any unbound secondary antibody with PBS twice for 5 min, the samples were incubated in a 1:200 dilution of the streptavidin–alkaline phosphatase complex and were further incubated in a *p*-nitrophenyl phosphate solution (Sigma). The optical density was measured at 405 nm wavelength.

Supporting Information

Supporting Information is available from the Wiley Online Library or from the author.

Acknowledgements

We thank Mrs. Friedrich for SEM investigations. This work was supported by the Deutsche Forschungsgemeinschaft (SCHM1597/17-1 and MA534/24-1).

[1] S. Miyamoto, H. Teramoto, J. S. Gutkind, K. M. Yamada, *J. Cell Biol.* **1996**, *135*, 1633.
[2] F. G. Giancotti, E. Ruoslahti, *Science* **1999**, *285*, 1028.
[3] R. S. Ross, *Cardiovasc. Res.* **2004**, *63*, 381.
[4] A. J. Engler, S. Sen, H. L. Sweeney, D. E. Discher, *Cell* **2006**, *126*, 677.
[5] M. Larsen, V. V. Artym, J. A. Green, K. M. Yamada, *Curr. Opin. Cell Biol.* **2006**, *18*, 463.
[6] V. Zwilling, E. Darque-Ceretti, A. Bautrry-Forveille, *Electrochim. Acta* **1999**, *45*, 921.
[7] K. C. Popat, K. I. Chatvanichkul, G. L. Barnes, T. J. Latempa Jr., C. A. Grimes, T. A. Desai, *J. Biomed. Mater. Res. A* **2006**, *6*, 955.
[8] M. J. Dalby, M. O. Riehle, S. J. Yarwood, C. D. Wilkinson, A. S. Curtis, *Exp. Cell Res.* **2003**, *284*, 274.
[9] M. Arnold, E. A. Cavalcanti-Adam, R. Glass, J. Blummel, W. Eck, M. Kantlehner, H. Kessler, J. P. Spatz, *ChemPhysChem* **2004**, *5*, 383.
[10] E. A. Cavalcanti-Adam, T. Volberg, A. Micoulet, H. Kessler, B. Geiger, J. P. Spatz, *Biophys. J.* **2007**, *92*, 2964.
[11] K. von der Mark, J. Park, S. Bauer, P. Schmuki, *Cell Tissue Res.* **2010**, *339*, 131.
[12] M. P. Lutolf, J. A. Hubbell, *Nat. Biotechnol.* **2005**, *23*, 47.
[13] A. E. X. Brown, D. Discher, *Curr. Biol.* **2009**, *19*, 781.
[14] J. Park, S. Bauer, K. von der Mark, P. Schmuki, *Nano Lett.* **2007**, *7*, 1686.
[15] J. Park, S. Bauer, K. A. Schlegel, F. W. Neukam, K. von der Mark, P. Schmuki, *Small* **2009**, *5*, 666.
[16] S. Bauer, J. Park, J. Faltenbacher, S. Berger, K. von der Mark, P. Schmuki, *Integr. Biol.* **2009**, *1*, 525.
[17] J. E. Aubin, F. Liu, L. Malaval, A. K. Gupta, *Bone* **1995**, *17*, 77S.
[18] A. Yamaguchi, T. Komori, T. Suda, *Endocr. Rev.* **2000**, *21*, 393.
[19] F. J. Hughes, W. Turner, G. Belibasakis, G. Martuscelli, *Periodontol. 2000* **2006**, *41*, 48.
[20] P. Chen, J. L. Carrington, R. G. Hammonds, A. H. Reddi, *Exp. Cell Res.* **1991**, *195*, 509.
[21] C. Shukunami, Y. Ohta, M. Sakuda, Y. Hiraki, *Exp. Cell Res.* **1998**, *241*, 1.
[22] T. C. Lindholm, T. S. Lindholm, A. Marttinen, M. R. Urist, *Clin. Orthop. Relat. Res.* **1994**, *301*, 263.
[23] R. S. Sellers, R. Zhang, S. S. Glasson, H. D. Kim, D. Peluso, D. A. D'Augusta, K. Beckwith, E. A. Morris, *J. Bone Joint Surg. Am.* **2000**, *82*, 151.
[24] S. Govender, C. Csimma, H. K. Genant, A. Valentin-Opran, Y. Amit, R. Arbel, H. Aro, D. Atar, M. Bishay, M. G. Borner, *J. Bone Joint Surg. Am.* **2002**, *84A*, 2123.
[25] K. Gelse, K. von der Mark, T. Aigner, J. Park, H. Schneider, *Arthritis Rheum.* **2003**, *48*, 430.
[26] J. Park, J. Ries, K. Gelse, F. Kloss, K. von der Mark, J. Wiltfang, F. W. Neukam, H. Schneider, *Gene Ther.* **2003**, *10*, 1089.
[27] T. J. Sigurdsson, E. Fu, D. N. Tatakis, M. D. Rohrer, U. M. Wikesjo, *Clin. Oral Implants Res.* **1997**, *8*, 367.
[28] K. Bessho, D. L. Carnes, R. Cavin, H. Y. Chen, J. L. Ong, *Clin. Oral Implants Res.* **1999**, *10*, 212.
[29] N. Sykaras, R. G. Triplett, M. E. Nunn, A. M. Iacopino, L. A. Opperman, *Clin. Oral Implants Res.* **2001**, *12*, 339.
[30] L. A. Salata, V. Franke-Stenport, L. Rasmusson, *Clin. Implant Dent. Relat. Res.* **2002**, *4*, 27.

[31] J. Park, R. Lutz, E. Felszeghy, J. Wiltfang, E. Nkenke, F. W. Neukam, K. A. Schlegel, *Biomaterials* **2007**, *28*, 2772.
[32] M. D. Pierschbacher, E. Ruoslahti, *Nature* **1984**, *309*, 30.
[33] B. K. Brandley, R. L. Schnaar, *Anal. Biochem.* **1988**, *172*, 270.
[34] J. Park, S. Bauer, K. von der Mark, P. Schmuki, *Nano Lett.* **2009**, *9*, 3157.
[35] A. S. G. Curtis, N. Gadegaard, M. J. Dalby, M. O. Riehle, C. D. W. Wilkinson, G. Aitchison, *IEEE Trans. Nanobiosci.* **2004**, *3*, 61.
[36] M. J. Dalby, D. McCloy, M. Robertson, H. D. Agheli, S. Affrossman, R. O. Oreffo, *Biomaterials* **2006**, *27*, 2980.
[37] K. Sugimori, K. Matsui, H. Motomura, T. Tokoro, J. Wang, S. Higa, T. Kimura, I. Kitajima, *J. Bone Miner. Metab.* **2005**, *23*, 411.
[38] Z. Liu, J. Shen, K. Pu, H. A. Katus, F. Plöger, C. P. Tiefenbacher, X. Chen, T. Braun, *Biochim. Biophys. Acta* **2009**, *1793*, 1819.
[39] S. A. Oberlender, R. S. Tuan, *Development* **1994**, *120*, 177.
[40] E. Canalis, A. N. Economides, E. Gazzerro, *Endocr. Rev.* **2003**, *24*, 218.
[41] R. Pogue, K. Lyons, *Curr. Top. Dev. Biol.* **2006**, *76*, 1.
[42] M. Wan, X. Cao, *Biochem. Biophys. Res. Commun.* **2005**, *328*, 651.
[43] R. E. Godin, E. J. Robertson, A. T. Dudley, *Int. J. Dev. Biol.* **1999**, *43*, 405.
[44] L. Dale, C. M. Jones, *Bioessays* **1999**, *21*, 751.
[45] P. D. Benya, J. D. Shaffer, *Cell* **1982**, *30*, 215.
[46] H. J. Häuselmann, M. B. Aydelotte, B. L. Schumacher, K. E. Kuettner, S. H. Gitelis, E. J.-M. A. Thonar, *Matrix* **1992**, *12*, 116.
[47] H. Chajra, C. F. Rousseau, D. Cortial, M. C. Ronziere, D. Herbage, F. Mallein-Gerin, A. M. Freyria, *Biomed. Mater. Eng.* **2008**, *18*, S33.
[48] P. Thorogood, *Development* **1983**, *2*, 223.
[49] B. K. Hall, *J. Embryol. Exp. Morphol.* **1980**, *58*, 251.
[50] R. Mayne, M. S. Vail, E. J. Miller, *Proc. Natl. Acad. Sci. USA* **1975**, *72*, 4511.
[51] K. von der Mark, V. Gauss, H. von der Mark, P. Mueller, *Nature* **1977**, *267*, 531.
[52] P. D. Benya, S. R. Padilla, M. E. Nimni, *Cell* **1978**, *15*, 1313.
[53] P. C. Marchisio, O. Capasso, L. Nitsch, R. Cancedda, E. Gionti, *Exp. Cell Res.* **1984**, *151*, 332.
[54] P. D. Benya, P. D. Brown, S. R. Padilla, *J. Cell Biol.* **1988**, *106*, 161.
[55] J. Dürr, S. Goodman, A. Potocnik, H. von der Mark, K. von der Mark, *Exp. Cell Res.* **1993**, *207*, 235.
[56] M. Enomoto, P. S. Leboy, A. S. Menko, D. Boettiger, *Exp. Cell Res.* **1993**, *205*, 276.
[57] R. F. Loeser, *Biorheology* **2002**, *39*, 119.
[58] P. Roy, S. Berger, P. Schmuki, *Angew. Chem., Int. Ed.* **2011**, *50*, 2904.
[59] S. Bauer, S. Kleber, P. Schmuki, *Electrochem. Commun.* **2006**, *8*, 1321.
[60] A. Ghicov, P. Schmuki, *Chem. Commun.* **2009**, *20*, 2791.
[61] J. P. Spatzin, *Nanobiotechnology* (Eds: C. M. Niemeyer, C. A. Mirkin), Wiley-VCH, Weinheim, **2004**, Chap. 4.
[62] J. M. Curran, R. Stokes, E. Irvine, D. Graham, N. A. Amro, R. G. Sanedrin, H. Jamilc, J. A. Hunta, *Lab Chip* **2010**, *10*, 1662.
[63] M. S. Killian, V. Wagener, P. Schmuki, S. Virtanen, *Langmuir* **2010**, *26*, 12044.
[64] M. S. Wagner, D. G. Castner, *Langmuir* **2001**, *17*, 4649.
[65] M. Henry, P. Bertrand, *Surf. Interface Anal.* **2009**, *41*, 105.
[66] M. R. Keenan, P. G. Kotula, *Surf. Interface Anal.* **2004**, *36*, 203.
[67] J. Park, V. Setter, V. Wixler, H. Schneider, *Tissue Eng. Part A* **2009**, *15*, 397.
[68] Y. Jiang, B. N. Jahagirdar, R. L. Reinhardt, R. E. Schwartz, C. D. Keene, X. R. Ortiz-Gonzalez, M. Reyes, T. Lenvik, T. Lund, M. Blackstad, J. Du, S. Aldrich, A. Lisberg, W. C. Low, D. A. Largaespada, C. M. Verfaillie, *Nature* **2002**, *418*, 41.

Received: April 22, 2011
Revised: August 8, 2011
Published online: November 18, 2011